Direct Solution Synthesis of Intermetallic AuCu and $AuCu_3$ Nanocrystals and Nanowire Networks

Amandeep K. Sra, Trevor D. Ewers, and Raymond E. Schaak*

Department of Chemistry, Texas A&M University, College Station, Texas 77842-3012

Received September 9, 2004. Revised Manuscript Received October 26, 2004

A modified polyol process has been used to synthesize intermetallic nanocrystals and nanowire networks directly in solution using a one-pot reaction. The synthesis of AuCu nanocrystals in tetraethylene glycol shows that atomically ordered intermetallic nanocrystals form above 250 °C, while atomically disordered alloy nanocrystals form at lower temperatures. The particle size increases with increasing solvent temperature, and there is a gradual shift from spherical to ellipsoidal morphology. Fully ordered intermetallic AuCu nanocrystals synthesized at 310 °C have an average particle width and height of 10 ± 3 and 8 ± 2 nm, respectively, and exist with faceted ellipsoidal, hexagonal, and cubic shapes. Replacing tetraethylene glycol with ethylene glycol, diethylene glycol, triethylene glycol, and glycerol yields highly branched nanowire networks. The morphology of the nanowire networks remains the same for all of the solvents, but the structure can be tuned from fully disordered alloy to fully ordered intermetallic AuCu, based on the boiling point of the solvent. The nanowire networks synthesized in ethylene glycol show that they likely form through a nanoparticle coalescence mechanism. By changing the stoichiometry of Au and Cu in solution, intermetallic $AuCu_3$ nanocrystals and nanowire networks can also be synthesized using tetraethylene glycol and glycerol, respectively. These results establish that it is possible to simultaneously control the structure, size, shape, and composition of intermetallic nanocrystals using solution chemistry, which has important implications for both fundamental scientific studies and future technological applications.

Introduction

Controlling the synthesis of inorganic nanocrystals is an important prerequisite for advancing nanotechnological applications, and also for understanding the fundamental interrelationships among structure, properties, and size in the nanometer size regime.[1,2] Significant progress has been made in this area in the past few years, and the ability to correlate the structures and morphologies of nanocrystals with physical properties is yielding a new level of understanding and is opening the door to new structures, properties, device configurations, and technologies.[3−7] Multimetallic solid-state materials, including alloys and intermetallic compounds, are especially intriguing as nanocrystals, as they are expected to play a pivotal role in many future applications. For example, intermetallic FePt nanocrystals are ferromagnetic with high coercivity and high magnetic anisotropy and are promising candidates for future high-density magnetic storage devices.[8] Likewise, many alloy nanoparticles are known to be highly active catalysts,[9−11] and several related intermetallic compounds show high catalytic activity as bulk materials and are predicted to be excellent candidates for nanoscale catalysts.[12−15]

Most of the successful strategies for synthesizing high-quality nanocrystals with controlled shape and size focus on semiconducting quantum dots,[6,16] oxides,[17−19] sulfides,[20−22]

* Corresponding author. Phone: (979) 458-2858. Fax: (979) 845-4719. E-mail: schaak@mail.chem.tamu.edu.

(1) Murray, C. B.; Kagan, C. R.; Bawendi, M. G. *Annu. Rev. Mater. Sci.* **2000**, *30*, 545−610.
(2) Alivisatos, A. P. *Science* **1996**, *271*, 933−937.
(3) (a) Ahmadi, T. S.; Wang, Z. L.; Green, T. C.; Henglun, A.; El-Sayed, M. A. *Science* **1996**, *272*, 1924−1926. (b) El-Sayed, M. A. *Acc. Chem. Res.* **2004**, *37*, 326−333. (c) Narayanan, R.; El-Sayed, M. A. *J. Am. Chem. Soc.* **2004**, *126*, 7194−7195.
(4) (a) Black, C. T.; Murray, C. B.; Sandstrom, R. L.; Sun, S. *Science* **2000**, *290*, 1131−1134. (b) Zeng, H.; Li, J.; Liu, J. P.; Wang, Z. L.; Sun, S. *Nature* **2002**, *420*, 395−398.
(5) Redl, F. X.; Cho, K. S.; Murray, C. B.; O'Brien, S. *Nature* **2003**, *423*, 968−971.
(6) Peng, X. *Adv. Mater.* **2003**, *15*, 459−463.
(7) Hyeon, T. *Chem. Commun.* **2003**, 927−934.
(8) Sun, S.; Murray, C. B.; Weller, D.; Folks, L.; Moser, A. *Science* **2000**, *287*, 1989−1992.
(9) Roucoux, A.; Schulz, J.; Patin, H. *Chem. Rev.* **2002**, *102*, 3757−3778.
(10) Scott, R. W. J.; Datye, A. K.; Crooks, R. M. *J. Am. Chem. Soc.* **2003**, *125*, 3708−3709.
(11) Chung, Y.-M.; Rhee, H.-K. *Catal. Lett.* **2003**, *85*, 159−164.
(12) (a) Casado-Rivera, E.; Gal, Z.; Angelo, A. C. D.; Lind, C.; DiSalvo, F. J.; Abruna, H. D. *Chem. Phys. Chem.* **2003**, *4*, 193−199. (b) Casado-Rivera, E.; Volpe, D. J.; Alden, L.; Lind, C.; Downie, C.; Vazquez-Alvarez, T.; Angelo, A. C. D.; DiSalvo, F. J.; Abruna, H. D. *J. Am. Chem. Soc.* **2004**, *126*, 4043−4049.
(13) Xu, Y.; Ruban, A. V.; Mavrikakis, M. *J. Am. Chem. Soc.* **2004**, *126*, 4717−4725.
(14) Xiong, L.; Manthiram, A. *J. Mater. Chem.* **2004**, *14*, 1454−1460.
(15) (a) Zhang, C. J.; Baxter, R. J.; Hu, P.; Alavi, A.; Lee, M.-H. *J. Chem. Phys.* **2001**, *115*, 5272−5277. (b) Mathauser, A. T.; Teplyakov, A. V. *Catal. Lett.* **2001**, *73*, 207−210.
(16) (a) Manna, L.; Scher, E. C.; Alivisatos, A. P. *J. Am. Chem. Soc.* **2000**, *122*, 12700−12706. (b) Scher, E. C.; Manna, L.; Alivisatos, A. P. *Philos. Trans. R. Soc. London, Ser. A* **2003**, *361*, 241−257. (c) Milliron, D. J.; Hughes, S. M.; Cui, Y.; Manna, L.; Li, J.; Wang, L.-W.; Alivisatos, A. P. *Nature* **2004**, *430*, 190−195.
(17) (a) Cozzoli, P. D.; Kornowski, A.; Weller, H. *J. Am. Chem. Soc.* **2003**, *125*, 14539−14548. (b) Jun, Y.-W.; Casula, M. F.; Sim, J.-H.; Kim, S. Y.; Cheon, J.; Alivisatos, A. P. *J. Am. Chem. Soc.* **2003**, *125*, 15981−15985.
(18) Cheon, J.; Kang, N.-J.; Lee, S.-M.; Lee, J.-H.; Yoon, J.-H.; Oh, S. J. *J. Am. Chem. Soc.* **2004**, *126*, 1950−1951.
(19) Song, Q.; Zhang, Z. J. *J. Am. Chem. Soc.* **2004**, *126*, 6164−6168.

10.1021/cm0484450 CCC: $30.25
Published on Web 01/26/2005

and simple metals.[23−29] As far as multimetallic materials are concerned, many examples of alloy nanoparticles are known,[30−39] but intermetallic nanocrystals are rare. Intermetallic FePt nanocrystals are routinely synthesized,[8,40−42] and intermetallic CoPt[43,44] and FePd[43] nanocrystals have been reported. However, the ordered intermetallic structures are only accessible after high-temperature transformations of deposited alloy nanoparticles. Such postsynthesis conversion often leads to irreversible sintering. Most other examples of intermetallic nanocrystals involve mechanical methods such as ball milling,[45] which yield polydisperse and irregularly shaped particles, or vacuum deposition and evaporation methods,[46] which are limited to planar supported films. No direct solution routes exist for synthesizing well-defined intermetallic nanocrystals, which limits future applications and scientific studies of this important class of solid-state materials.

We recently reported a new multistep approach for synthesizing solution-dispersible intermetallic nanocrystals of AuCu and $AuCu_3$.[47,48] This strategy relies on binary nanocomposite precursors that are annealed in powder form to induce interdiffusion and nucleation at low temperatures. The low-temperature processing and polymer stabilization minimize sintering, and the nanocrystals can be readily redispersed back into solution. While this approach yields excellent control over composition and structure, it tends to form polydisperse nanocrystals with irregular shapes, and as such is not generally amenable to size and shape control because of the powder processing step. Such nanocrystals are appropriate for some applications (e.g., catalysis and reinforced structural nanocomposites), but intermetallic nanocrystals with controlled shape and size are necessary for device integration and fundamental structure−property studies.

The Au−Cu system is an ideal target for developing new nanocrystal synthetic routes. In bulk systems, the Au−Cu binary phase diagram is well understood, and several distinct intermetallic phases are known.[49] In particular, AuCu and $AuCu_3$ are textbook-type models of order/disorder phase transitions in solids, and many other important intermetallic compounds adopt these structure types.[50] Several theoretical studies have addressed the structure and ordering of Au and Cu in binary clusters,[51] and numerous theoretical predictions concerning equilibrium composition distributions,[52] phase separation,[53] surface segregation,[52,54] and nanocrystal shape[39d,55]

(20) (a) Jun, Y.-W.; Jung, Y.-Y.; Cheon, J. *J. Am. Chem. Soc.* **2002**, *124*, 615−619. (b) Lee, S.-M.; Jun, Y.-W.; Cho, S.-N.; Cheon, J. *J. Am. Chem. Soc.* **2002**, *124*, 11244−11245.
(21) Joo, J.; Na, H. B.; Yu, T.; Yu, J. H.; Kim, Y. W.; Wu, F.; Zhang, J. Z.; Hyeon, T. *J. Am. Chem. Soc.* **2003**, *125*, 11100−11105.
(22) (a) Sigman, M. B.; Ghezelbash, A.; Hanrath, T.; Saunders, A. E.; Lee, F.; Korgel, B. A. *J. Am. Chem. Soc.* **2003**, *125*, 16050−16057. (b) Ghezelbash, A.; Sigman, M. B.; Korgel, B. A. *Nano Lett.* **2004**, *4*, 537−542.
(23) Puntes, V. F.; Krishnan, K. M.; Alivisatos, A. P. *Science* **2001**, *291*, 2115−2117.
(24) Sun, Y.; Xia, Y. *Science* **2002**, *298*, 2176−2179.
(25) (a) Jin, R.; Cao, Y.; Mirkin, C. A.; Kelly, K. L.; Schatz, G. C.; Zheng, J. G. *Science* **2001**, *294*, 1901−1903. (b) Jin, R.; Cao, Y. C.; Hao, E.; Metraux, G. S.; Schatz, G. C.; Mirkin, C. A. *Nature* **2003**, *425*, 487−490. (c) Maillard, M.; Huang, P.; Brus, L. *Nano Lett.* **2003**, *3*, 1611−1615. (d) Callegari, A.; Tonti, D.; Chergui, M. *Nano Lett.* **2003**, *3*, 1565−1568.
(26) (a) Chen, S.; Wang, Z. L.; Ballato, J.; Foulger, S. H.; Carroll, D. L. *J. Am. Chem. Soc.* **2003**, *125*, 16186−16187. (b) Hao, E.; Bailey, R. C.; Schatz, G. C.; Hupp, J. T.; Li, S. *Nano Lett.* **2004**, *4*, 327−330.
(27) (a) Murphy, C. J.; Jana, N. R. *Adv. Mater.* **2002**, *14*, 80−82. (b) Sau, T. K.; Murphy, C. J. *J. Am. Chem. Soc.* **2004**, *126*, 8648−8649.
(28) Dumestre, F.; Chaudret, B.; Amiens, C.; Renaud, P.; Fejes, P. *Science* **2004**, *303*, 821−823.
(29) Kim, F.; Connor, S.; Song, H.; Kuykendall, T.; Yang, P. *Angew. Chem., Int. Ed.* **2004**, *43*, 3673−3677.
(30) (a) Stahl, B.; Gajbhiye, N. S.; Wilde, G.; Kramer, D.; Ellrich, J.; Ghafari, M.; Hahn, H.; Gleiter, H.; Weissmuller, J.; Wurschum, R.; Schlossmacher, P. *Adv. Mater.* **2002**, *14*, 24−27. (b) Elkins, K. E.; Vedantam, T. S.; Liu, J. P.; Zeng, H.; Sun, S.; Ding, Y.; Wang, Z. L. *Nano Lett.* **2003**, *3*, 1647−1649. (c) Liu, C.; Wu, X.; Klemmer, T.; Shukla, N.; Yang, X.; Weller, D.; Roy, A. G.; Tanase, M.; Laughlin, D. *J. Phys. Chem. B* **2004**, *108*, 6121−6123. (d) Chen, M.; Liu, J. P.; Sun, S. *J. Am. Chem. Soc.* **2004**, *126*, 8394−8395.
(31) Sun, S.; Anders, S.; Thomson, T.; Baglin, J. E. E.; Toney, M. F.; Hamann, H. F.; Murray, C. B.; Terris, B. D. *J. Phys. Chem. B* **2003**, *107*, 5419−5425.
(32) Teng, X.; Yang, H. *J. Am. Chem. Soc.* **2003**, *125*, 14559−14563.
(33) (a) Santra, A. K.; Subanna, G. N.; Rao, C. N. R. *Surf. Sci.* **1994**, *317*, 259−268. (b) Harikumar, K. R.; Ghosh, S.; Rao, C. N. R. *J. Phys. Chem. A* **1997**, *101*, 536−540.
(34) Liz-Marzan, L. M.; Philipse, A. P. *J. Phys. Chem.* **1995**, *99*, 15120−15128.
(35) Nashner, M. S.; Frenkel, A. I.; Adler, D. L.; Shapley, J. R.; Nuzzo, R. G. *J. Am. Chem. Soc.* **1997**, *119*, 7760−7771.
(36) Hostetler, M. J.; Zhong, C.-J.; Yen, B. K. H.; Anderegg, J.; Gross, S. M.; Evans, N. D.; Porter, M.; Murray, R. W. *J. Am. Chem. Soc.* **1998**, *120*, 9396−9397.
(37) Link, S.; Wang, Z. L.; El-Sayed, M. A. *J. Phys. Chem. B* **1999**, *103*, 3529−3533.
(38) Park, J.-I.; Cheon, J. *J. Am. Chem. Soc.* **2001**, *123*, 5743−5746.
(39) Fang, J.; Tung, L. D.; Stokes, K. L.; He, J.; Caruntu, D.; Zhou, W. L.; O'Connor, C. J. *J. Appl. Phys.* **2002**, *91*, 8816−8818.
(40) (a) Ely, T. O.; Pan, C.; Amiens, C.; Chaudret, B.; Dassenoy, F.; Lecante, P.; Casanove, M.-J.; Mosset, A.; Respaud, M.; Broto, J.-M. *J. Phys. Chem. B* **2000**, *104*, 695−702. (b) Zitoun, D.; Amiens, C.; Chaudret, B.; Fromen, M.-C.; Lecante, P.; Casanove, M.-J.; Respaud, M. *J. Phys. Chem. B* **2003**, *107*, 6997−7005.
(41) (a) Shevchenko, E. V.; Talapin, D. V.; Rogach, A. L.; Kornowski, A.; Haase, M.; Weller, H. *J. Am. Chem. Soc.* **2002**, *124*, 11480−11485. (b) Shevchenko, E. V.; Talapin, D. V.; Schnablegger, H.; Kornowski, A.; Festin, O.; Svedlindh, P.; Haase, M.; Weller, H. *J. Am. Chem. Soc.* **2003**, *125*, 9090−9101.
(42) (a) Sangregorio, C.; Galeotti, M.; Bardi, U.; Baglioni, P. *Langmuir* **1996**, *12*, 5800−5802. (b) Gwak, J. H.; Kim, S.-J.; Lee, M. *J. Phys. Chem. B* **1998**, *102*, 7699−7704. (c) Kim, M. J.; Na, H.-J.; Lee, K. C.; Yoo, E. A.; Lee, M. *J. Mater. Chem.* **2003**, *13*, 1789−1792. (d) Pal, U.; Sanchez Ramirez, J. F.; Liu, H. B.; Medina, A.; Ascencio, J. A. *Appl. Phys. A* **2004**, *79*, 79−84. (e) Gwak, J.-H.; Kim, S.-J.; Lee, M. *J. Phys. Chem. B* **1998**, *102*, 7699−7704.
(43) Chen, M.; Nikles, D. E. *J. Appl. Phys.* **2002**, *91*, 8477−8480.
(44) (a) Yu, A. C. C.; Mizuno, M.; Sasaki, Y.; Kondo, H.; Hiraga, K. *Appl. Phys. Lett.* **2002**, *81*, 3768−3771. (b) Park, J.-I.; Kiml, M. G.; Jun, Y.-W.; Lee, J. S.; Lee, W.-R.; Cheon, J. *J. Am. Chem. Soc.* **2004**, *126*, ASAP Article.
(45) (a) Koch, C. C. *Nanostruct. Mater.* **1997**, *9*, 13−22. (b) Suryanarayana, C.; Ivanov, E.; Boldyrev, V. V. *Mater. Sci. Eng., A* **2001**, *304−306*, 151−158.
(46) (a) Sato, K.; Bian, B.; Hirotsu. *Jpn. J. Appl. Phys.* **2000**, *39*, L1121−L1123. (b) Takahashi, Y. K.; Koyama, T.; Ohnuma, M.; Ohkubo, T.; Hono, K. *J. Appl. Phys.* **2004**, *95*, 2690−2696.
(47) Sra, A. K.; Schaak, R. E. *J. Am. Chem. Soc.* **2004**, *126*, 6667−6672.
(48) Schaak, R. E.; Sra, A. K.; Leonard, B. M.; Cable, R. E.; Bauer, J. C.; Han, Y.-F.; Means, J.; Teizer, W.; Vasquez, Y.; Funck, E. S. *J. Am. Chem. Soc.* **2005**, in press.
(49) Massalski, T. B., Ed.; *Binary Alloy Phase Diagrams*; ASM International: Materials Park, OH, 1996.
(50) Villars, P., Calvert, L. D., Eds.; *Pearson's Handbook of Crystallographic Data for Intermetallic Phases*, 2nd ed.; ASM International: Materials Park, OH, 1991.
(51) (a) Lopez, M. J.; Marcos, P. A.; Alonso, J. A. *J. Chem. Phys.* **1996**, *104*, 1056−1066. (b) Darby, S.; Mortimer-Jones, T. V.; Johnston, R. L.; Roberts, C. *J. Chem. Phys.* **2002**, *116*, 1536−1550. (c) Lordeiro, R. A.; Guimaraes, F. F.; Belchior, J. C.; Johnston, R. L. *Int. J. Quantum Chem.* **2003**, *95*, 112−125. (d) Rodriguez-Lopez, J. L.; Montejano-Carrizales, J. M.; Jose-Yacaman, M. *Appl. Surf. Sci.* **2003**, *219*, 56−63.
(52) Wilson, N. T.; Johnston, R. L. *J. Mater. Chem.* **2002**, *12*, 2913−2922.

have been reported. Furthermore, one study of the order/disorder phase transition in AuCu and $AuCu_3$ nanocrystals demonstrated a suppression of the ordering temperature with decreasing particle size for lithographically fabricated nanoislands,[56] and another study showed that a critical size exists for atomic ordering in Au−Cu nanoparticles.[57] Clearly, the availability of high-quality chemically synthesized intermetallic AuCu and $AuCu_3$ nanoparticles will be critical for unraveling the size-dependence of a variety of fundamental physical phenomena, as well as to test the theories that have been proposed for the model Au−Cu system.

Interestingly, while uniform nanocrystals of atomically disordered AuCu and $AuCu_3$ alloys have been reported by several groups,[39] no direct solution routes to analogous intermetallic nanocrystals exist. From our previous work with 15−30 nm AuCu and $AuCu_3$ nanocrystals synthesized from binary nanocomposite precursors, we observed that nucleation of the ordered phases occurs at temperatures that are similar to those expected for bulk systems.[47,48] Solution routes, particularly the polyol process,[58,59] generally are more amenable to controlling nanocrystal size and shape than solvent-free syntheses. Recognizing that the nucleation temperatures for intermetallic AuCu and $AuCu_3$ (200−300 °C) fall within a temperature range accessible using high-boiling solvents,[49] we speculated that it would be possible to directly synthesize uniform intermetallic nanocrystals in solution. Accordingly, we report here a modified polyol synthetic route to ordered intermetallic AuCu and $AuCu_3$ nanocrystals. By carefully matching solvent temperature to the binary equilibrium phase diagram, we show that appropriate conditions exist for stabilizing both alloy and intermetallic nanocrystals with controlled structures and shapes. Furthermore, under appropriate conditions, intermetallic nanowire networks can also be synthesized in a single step. This ability to simultaneously control structure, size, shape, and composition is unprecedented for intermetallic nanomaterials.

Experimental Section

Nanocrystals of AuCu were synthesized using a modification of the polyol process. $Cu(C_2H_3O_2)_2$ (6.8 mg), $HAuCl_4 \cdot 3H_2O$ (13.3 mg), and poly(vinylpyrrolidone) (PVP, MW = 630 000, 100 mg) were dissolved in 50 mL of tetraethylene glycol under sonication. After stirring under Ar for 20−30 min, 25 mL of freshly prepared 0.01 M $NaBH_4$ dissolved in tetraethylene glycol was added, and the solution was heated to reflux and held there for 15 min. After being cooled to room temperature, the AuCu nanocrystals were isolated by centrifugation, washed several times with ethanol to remove any excess polymer, and then dried under ambient conditions. The samples were resuspended in ethanol by sonicating 1 mg of nanocrystal powder in 2 mL of ethanol. $AuCu_3$ nanocrystals were prepared in a similar way, using 13.4 mg of $Cu(C_2H_3O_2)_2$ and 13.3 mg of $HAuCl_4 \cdot 3H_2O$ to yield a 2:1 ratio and refluxing for 30−60 min. AuCu nanowire networks were synthesized in a similar manner, using other high boiling solvents (ethylene glycol, diethylene glycol, triethylene glycol, and glycerol) instead of tetraethylene glycol.

Powder X-ray diffraction (XRD) data were collected on a Bruker GADDS three-circle X-ray diffractometer using Cu Kα radiation. High-resolution transmission electron microscopy (TEM), energy-dispersive X-ray spectroscopy (EDS), and selected area electron diffraction (SAED) data were collected on a JEOL JEM-2010 TEM. TEM samples were prepared by placing one drop of the resuspended nanocrystal solution onto a carbon-coated Cu grid, and allowing it to dry. Samples for EDS analysis were deposited onto a Ni grid to avoid erroneously detecting Cu from the traditional Cu grids.

Results and Discussion

Synthesis of Intermetallic AuCu Nanocrystals. In our previous work, binary Au−Cu nanocomposites were sequentially converted into AuCu alloy and intermetallic nanocrystals by annealing them as powders.[47,48] We found that atomically disordered (alloy) AuCu formed by 175 °C and that ordered (intermetallic) AuCu began to form at 200 °C. Fully ordered AuCu was present by 300 °C. To study the temperature dependence of intermetallic nanocrystal formation in solution, we chose tetraethylene glycol (TEG, BP = 310 °C) as a high boiling solvent. The reagents [$Cu(C_2H_3O_2)$, $HAuCu_4 \cdot 3H_2O$, PVP] were first dissolved in TEG and reduced with $NaBH_4$ at room temperature, and then heated to a variety of temperatures between 100 and 310 °C to map out the phase behavior of their nanocrystal formation.

XRD data for AuCu nanocrystals synthesized in TEG at different temperatures are shown in Figure 1. At 150 °C, the XRD data show a single-phase face-centered cubic (fcc) pattern with $a = 3.88$ Å, which is contracted relative to Au ($a_{Au} = 4.078$ Å).[50] This indicates the formation of an alloy between Au and Cu. At 200 °C, the pattern still resembles a single fcc phase with $a = 3.84$ Å, consistent with the incorporation of more Cu into the Au_xCu_{1-x} alloy. Between 250 and 280 °C, weak superlattice reflections begin to appear, and these can be assigned to the tetragonal structure of intermetallic AuCu. By 290 °C, intermetallic AuCu is clearly formed, and the lattice constants ($a = 3.93$ Å, $c = 3.64$ Å) agree well with those expected for tetragonal AuCu ($a_{lit} = 3.963$ Å, $c_{lit} = 3.671$ Å).[50]

The degree of atomic ordering can be quantified using the chemical order parameter (S), which is determined from the ratio of the intensity of the superlattice peaks (*001* and *110*) to the fundamental peaks (e.g., *111*).[41,60] For a fully disordered alloy, $S = 0$, and for a fully ordered intermetallic, $S = 1$. Below 200 °C, no superlattice peaks are evident, so $S = 0$ and Au_xCu_{1-x} exists as an atomically disordered alloy. Between 250 and 290 °C, superlattice peaks are evident. However, the chemical order parameter, which is difficult

(53) Christensen, A.; Stoltze, P.; Norskov, J. K. *J. Phys.: Condens. Matter* **1995**, *7*, 1047−1057.
(54) Ruban, A. V.; Skriver, H. L.; Norksov, J. K. *Phys. Rev. B* **1999**, *59*, 15990−16000.
(55) (a) Rodriguez-Lopez, M. J.; Montejano-Carrizales, J. M.; Pal, U.; Sanchez-Ramirez, J. F.; Troiani, H. E.; Garcia, D.; Miki-Yoshida, M.; Jose-Yacaman, M. *Phys. Rev. Lett.* **2004**, *92*, 196102.
(56) Schulli, T.; Trenkler, J.; Monch, I.; LeBolloc, D.; Dosch, H. *Europhys. Lett.* **2002**, *58*, 737−743.
(57) (a) Tadaki, T.; Koreeda, A.; Nakata, Y.; Kinoshita, T. *Surf. Rev. Lett.* **1996**, *1*, 65−69. (b) Tadaki, T.; Kinoshita, T.; Nakata, Y.; Ohkubo, T.; Hirotsu. *Z. Phys. D: At., Mol. Clusters* **1997**, *40*, 493−495.
(58) Fievet, F.; Lagier, J. P.; Blin, B.; Beaudoin, B.; Figlarz, M. *Solid State Ionics* **1989**, *32/33*, 198−205.
(59) Murray, C. B.; Sun, S.; Gaschler, W.; Doyle, H.; Betley, T. A.; Kagan, C. R. *IBM J. Res. Dev.* **2001**, *45*, 47−56.
(60) Cebollada, A.; Farrow, R. F. C.; Toney, M. F. In *Magnetic Nanostructures*; Nalwa, H. S., Ed.; American Scientific Publishers: Stevenson Ranch, CA, 2002; p 93.

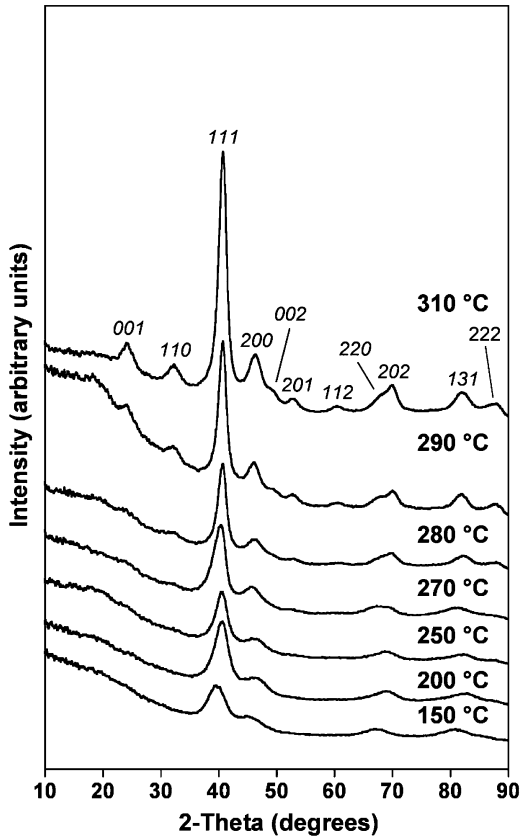

Figure 1. Powder XRD patterns for AuCu nanoparticles synthesized in tetraethylene glycol at a variety of temperatures.

to quantitate due to the weak superlattice peaks, ranges from 0.2 to 0.7. This clearly indicates that there is only partial ordering. At 310 °C, $S \approx 1$, which indicates long-range atomic ordering in intermetallic AuCu. These data indicate that solution synthesis using TEG as a solvent allows the structure to be systematically tuned between alloy and intermetallic phases.

Particle size analysis of the XRD data in Figure 1 using the Scherrer formula[61] for the *111* reflection shows that the crystallite size varies as a function of annealing temperature. At 150 °C, the average particle size is 2.9 nm, and it increases systematically to 9.3 nm by 310 °C. Some crystal growth is occurring as the temperature is increased. Some previous reports on intermetallic Au−Cu nanocrystals (synthesized as thin films using vacuum deposition or evaporation methods) suggested that there is a size dependence to nucleating the ordered phase,[56] and also that there may be a critical size, around 4 nm, below which ordering does not occur.[57] The data presented here suggest that ordering does not occur below 250 °C, which is a higher temperature than is necessary to induce ordering in nanocomposite powder samples with larger particle sizes. At the same time, the particle sizes for the disordered nanocrystals synthesized in TEG between 150 and 250 °C are below 5 nm, so if a critical size for ordering does exist, ordering may not be expected. Thus, the fact that we do not observe ordering below 250 °C is interesting and could possibly be a manifestation

(61) Klug, H. P.; Alexander, L. E. *X-ray Diffraction Procedures*; John Wiley: New York, 1959.

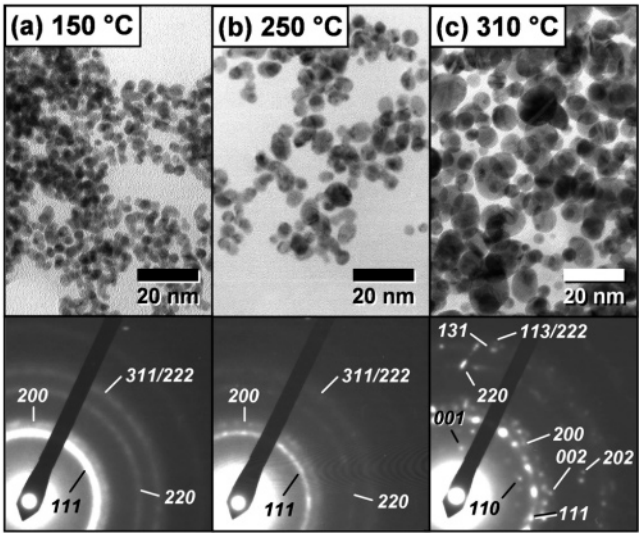

Figure 2. TEM micrographs and corresponding SAED patterns for AuCu nanocrystals synthesized in tetraethylene glycol at (a) 150 °C, (b) 250 °C, and (c) 310 °C.

of the predicted size-dependence of ordering. Of course, our data do not rigorously establish a size-dependence to ordering, because both the size and the structure change with temperature. Further synthetic optimization and purification to yield monodisperse nanocrystals will be critical for unraveling the nature of this phenomenon.

Representative TEM images of alloy and intermetallic AuCu nanocrystals are shown in Figure 2, along with their corresponding SAED patterns. AuCu nanocrystals synthesized at 150, 250, and 310 °C are shown in Figure 2a−c. The SAED patterns confirm that the AuCu nanocrystals synthesized at 150 and 250 °C are predominantly disordered alloys, which is consistent with the bulk XRD data in Figure 1. The SAED pattern of the AuCu nanocrystals synthesized at 310 °C confirms the atomic ordering that was observed in the XRD data. The reflections characteristic of the face-centered tetragonal structure of AuCu (*001*, *110*, *200*/*002*, *220*/*202*) are clearly visible in the SAED pattern. No impurities are detectible in either the XRD or the SAED data. EDS analysis on several intermetallic AuCu nanocrystals reveals an average composition of 45:55 (Au:Cu), which is within experimental error of the nominal 1:1 stoichiometry and also within the thermodynamic stability window for intermetallic AuCu based on the equilibrium phase diagram.[49]

The disordered AuCu alloy nanoparticles synthesized at 150 °C appear small, uniform, and generally spherical, although closer inspection indicates that many of the particles are elongated. The size distribution histogram in Figure 3a shows that the particles range in size from 3 to 7 nm. To quantify the ellipsoidal character of the nanoparticles, the width and height were considered separately to yield two-dimensional histogram data. For AuCu synthesized at 150 °C, the average nanoparticle widths and heights are 5.0 ± 1 and 4.6 ± 1 nm, respectively. These data show an overall spherical shape for the AuCu alloy nanoparticles. A two-dimensional particle size analysis for the AuCu nanocrystals synthesized at 250 °C is shown in Figure 3b. The average particle widths and heights are 7 ± 2 and 6 ± 1 nm, respectively. Although there is still not a significant

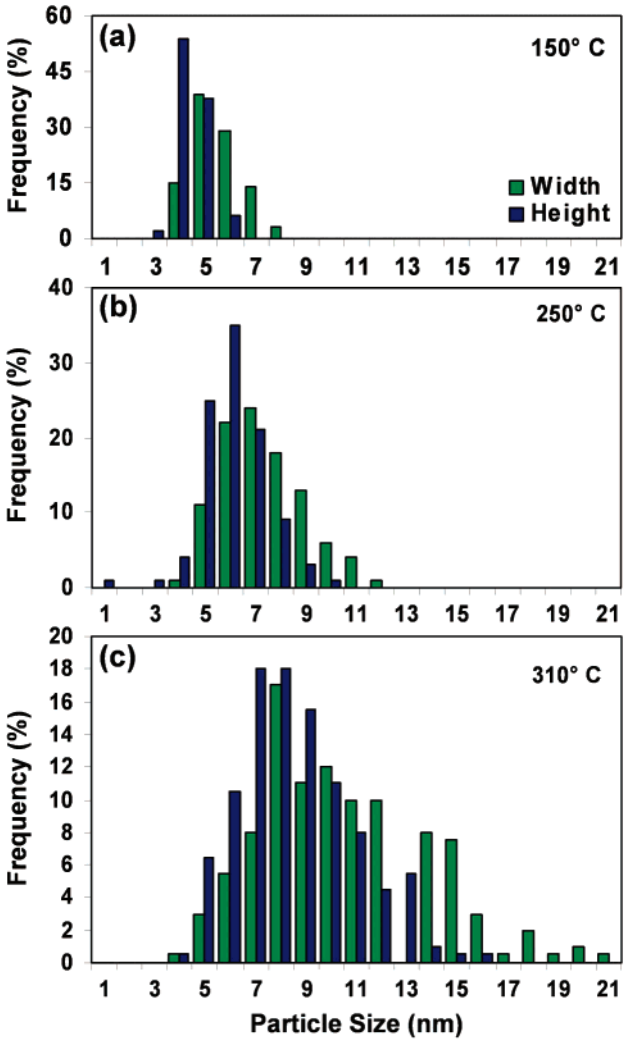

Figure 3. Particle size distribution histograms for AuCu nanocrystals synthesized in tetraethylene glycol at (a) 150 °C, (b) 250 °C, and (c) 310 °C. The width and height are plotted separately. The reported particle sizes and distributions (see text) are based on measurements of ca. 150 individual nanoparticles for each sample. Large regions of overlapping particles were not analyzed to avoid miscalculations.

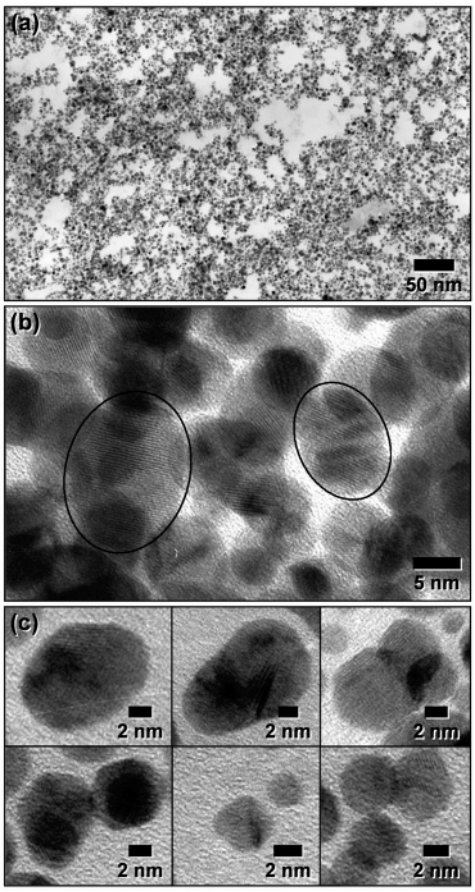

Figure 4. Low-resolution (a) and high-resolution (b) TEM micrographs of AuCu nanocrystals synthesized in tetraethylene glycol at 310 °C. Representative examples of individual nanocrystals are shown in (c) and include nanocrystals with remarkably straight edges, and others that adopt hexagonal and cubic shapes. Two ellipsoidal nanoparticles in (b) are outlined for clarity.

difference between the average widths and heights, the ellipsoidal distortion appears to increase slightly. The size distribution histogram for intermetallic AuCu nanocrystals synthesized at 310 °C (Figure 3c) shows that the size distribution is broader and that there is clearly a greater population of heights (relative to widths) at small particle sizes and the reverse at large particle sizes. While there is not a bimodal distribution, the average widths and heights (10 ± 3 and 8 ± 2 nm, respectively) suggest an overall ellipsoidal morphology for the intermetallic AuCu nanocrystals. A few ellipsoidal nanoparticles are outlined for clarity in Figure 4b. The average particle sizes determined by TEM analysis agree well with the crystallite sizes estimated from the bulk XRD data using the Scherrer equation, which suggests that a majority of the nanoparticles are single crystals.

The lattice fringes evident in the higher resolution TEM images in Figure 4b confirm that the nanoparticles are generally single crystals. Likewise, the low-resolution TEM image in Figure 4a highlights the overall monodispersity of the sample and the fact the nanoparticles are generally well-dispersed and not aggregated. (Apparent aggregation in some of the TEM images is primarily a result of TEM grid preparation.) Furthermore, Figure 4 shows that some of the nanocrystals are spherical, but many also adopt an ellipsoidal shape that is characterized by well-defined facets. Figure 4c, for example, shows representative nanocrystals that have remarkably straight edges, and others that adopt hexagonal and cubic morphologies. Several theoretical studies have addressed the issue of crystallite shape for AuCu nanocrystals.[51,55] The results in Figure 4 provide experimental evidence that intermetallic AuCu nanocrystals synthesized using chemical methods do indeed exist as faceted nanocrystals that are not uniformly spherical, although higher-resolution imaging will be necessary to directly observe twinning and more complex atomic arrangements within the individual nanocrystals.

Solutions of alloy nanoparticles tend to have optical absorption spectra that show a single plasmon band with a peak maximum that is intermediate between those of the monometallic species.[62] For Au−Cu alloy nanoparticles reported previously, the plasmon absorption maxima fall between that of Au (ca. 520 nm) and that of Cu (ca. 570 nm).[39] To our knowledge, optical absorption spectra

(62) (a) Mulvaney, P. *Langmuir* **1996**, *12*, 788−800. (b) Link, S.; Wang, Z. L.; El-Sayed, M. A. *J. Phys. Chem. B* **1999**, *103*, 3529−3533.

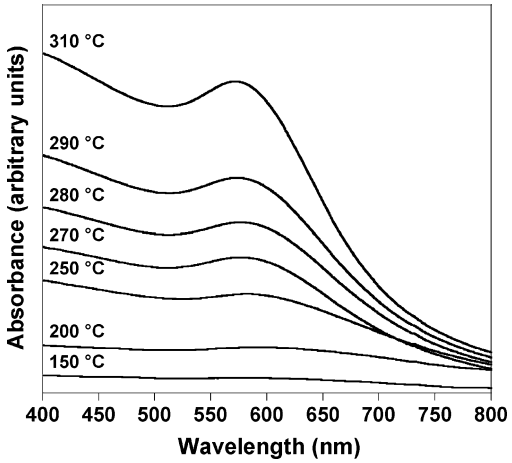

Figure 5. Visible absorption spectra for dilute solutions of AuCu nanoparticles synthesized in TEG at a variety of temperatures.

for intermetallic nanocrystals have not been studied in detail. Figure 5 shows the visible absorption spectra for AuCu nanoparticles synthesized in TEG at temperatures between 150 and 310 °C. All of the spectra show a single plasmon band, which confirms the formation of a single metallic nanocrystalline phase. For the lower-temperature samples, the plasmon band is significantly broadened, which is expected for the smallest particles.[62,63] This follows directly from theory, which describes broadening of the plasmon band as a function of decreasing particle size.[62,63] The increasing sharpness of the plasmon band with annealing temperature is also consistent with the particle size analysis, which shows that the nanoparticle sizes increase systematically with temperature. All of the absorption maxima are between 565 and 585 nm, which is significantly higher than the absorption maximum for Au nanoparticles, and near that expected for pure Cu nanoparticles.[39,63] The wavelengths of the absorption maxima are also higher than those reported for AuCu alloy nanoparticles synthesized at significantly lower temperatures (e.g., 548[39d] and ca. 560 nm[39c]). There is also a small blue shift in the absorption maxima as the annealing temperature increases. Interpreting these features is difficult, because many factors are known to shift the absorption maxima to higher and lower energies. Surface scattering effects and interactions of the solvent molecules and surface stabilizers with the metal particles are well-known to cause variable absorption spectra.[62a] Likewise, nanoparticle aggregation is known to cause a red-shift in the absorption maxima.[64,65] A report of AuCu alloy nanocrystals confined in a SiO_2 matrix also showed higher-wavelength absorption maxima (580−594 nm), and these absorption maxima shift to smaller wavelengths with increasing temperature.[39e] The reason for this is unknown and may be attributable to scattering, but nonetheless is consistent with our data. Regardless, the absorption features we observe (blue-shift with increasing temperature, superimposed on an overall red-shift due to some nanoparticle aggregation) are different than some literature reports, but are not without precedent, and they may be related to either the change in size, morphology, or aggregation state of the nanoparticles, or the influence of atomic ordering on the surface plasmon bands.

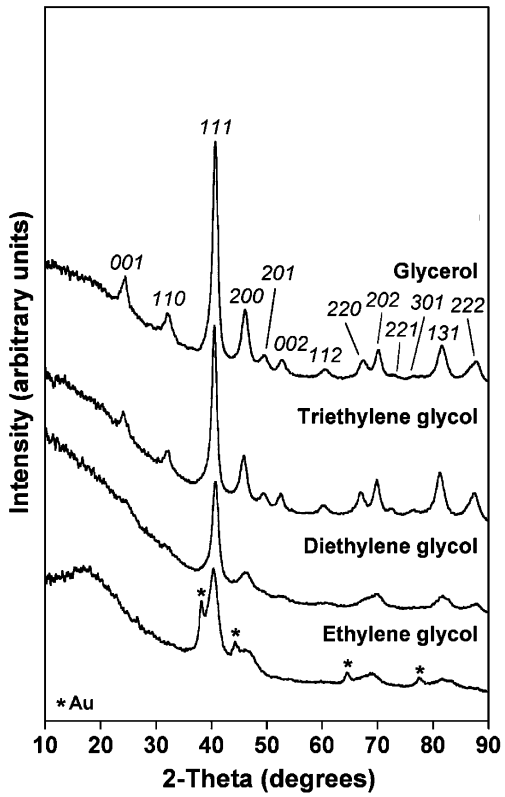

Figure 6. Powder XRD patterns for AuCu nanoparticles synthesized in ethylene glycol (198 °C), diethylene glycol (246 °C), triethylene glycol (285 °C), and glycerol (290 °C).

Synthesis of Intermetallic Nanowire Networks. TEG was initially used as a high-boiling solvent because it has a sufficiently high boiling point to allow us to carefully study the temperature-dependent formation of intermetallic AuCu nanocrystals without varying any other synthetic parameters. There are, however, a variety of solvents with intermediate boiling points in the temperature range we studied. For example, ethylene glycol (EG), diethylene glycol (DEG), triethylene glycol (TREG), and glycerol (GLY) have boiling points of 198, 246, 285, and 290 °C, respectively. Figure 6 shows XRD data for AuCu nanocrystals synthesized in the above solvents. AuCu synthesized in ethylene glycol (198 °C) yields a mixture of phases: Au and disordered AuCu alloy. (Refluxing for a longer time yields pure AuCu alloy, suggesting that the reaction kinetics are slower in ethylene glycol than in TEG or in other solvents at higher temperatures.) DEG (246 °C) yields nanocrystalline AuCu with some short-range ordering, indicating the onset of intermetallic formation. TREG (285 °C) and GLY (290 °C) yield fully ordered intermetallic AuCu ($S \approx 1$), as expected. These results are consistent with our earlier observations using TEG as a solvent (Figure 1).

TEM images and corresponding SAED patterns for nanocrystalline AuCu alloy and intermetallic phases synthesized in DEG, TREG, and GLY are shown in Figure 7. Surprisingly, discrete nanocrystals are not observed. Rather, highly interconnected and branched nanowire networks form in-

(63) Lisiecki, I.; Pileni, M. P. *J. Phys. Chem. B* **1995**, *99*, 5077−5082.
(64) Fleming, D. A.; Williams, M. E. *Langmuir* **2004**, *20*, 3021−3023.
(65) Ramanath, G.; D'Arcy-Gall, J.; Maddanimath, T.; Ellis, A. V.; Ganesan, P. G.; Goswami, R.; Kumar, A.; Vijayamohanan, K. *Langmuir* **2004**, *20*, 5583−5587.

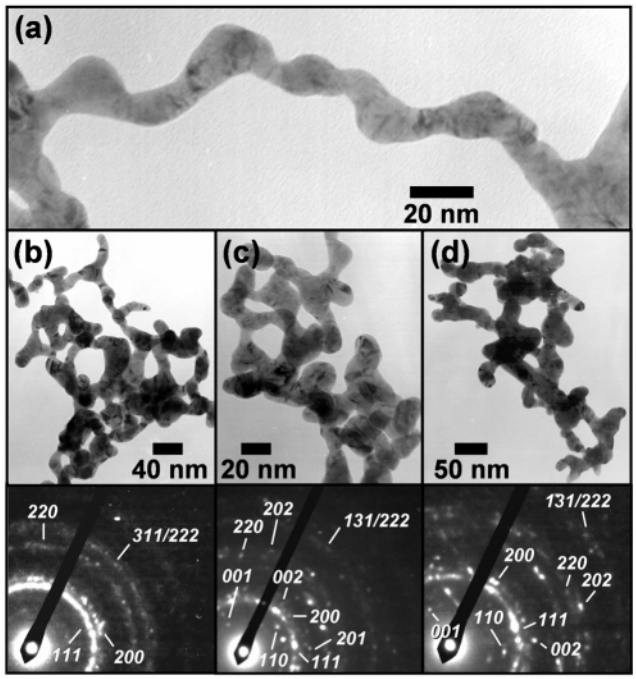

Figure 7. A TEM micrograph of an AuCu nanowire synthesized in diethylene glycol is shown in (a). TEM micrographs and corresponding SAED patterns for AuCu nanowire networks synthesized in diethylene glycol, triethylene glycol, and glycerol are shown in (b), (c), and (d), respectively.

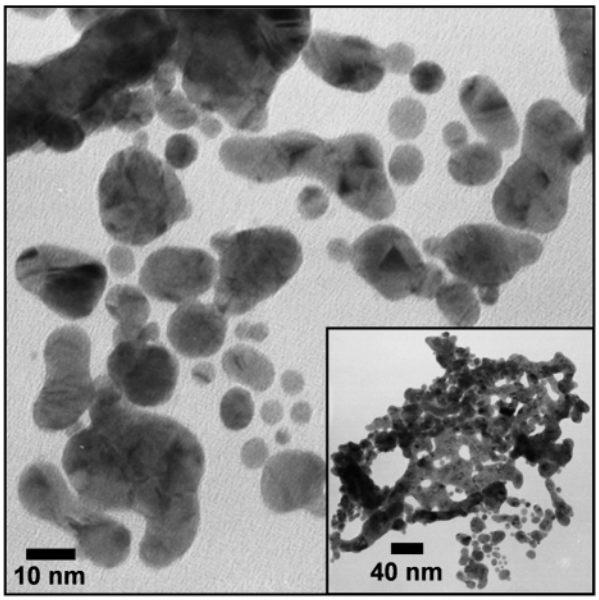

Figure 8. TEM micrographs of AuCu synthesized in ethylene glycol. The inset shows a highly branched AuCu nanowire network. The region of the nanowire network that is only partially formed is enlarged in the main panel, showing the coalescence of several smaller nanoparticles into an interconnected network.

stead. Interestingly, many of the nanowire networks exhibit three-fold branch points with spokes that are separated by 120°. An example of a 140 × 15 nm wire synthesized in DEG is shown in Figure 7a.

The SAED patterns show that the AuCu nanowire network formed in DEG is predominantly a disordered alloy, while those synthesized in TREG and GLY exist as the intermetallic form of AuCu. This indicates that the internal crystal structure of the nanowire networks can be systematically tuned from alloy to intermetallic with no change in morphology. The average diameters of the nanowires synthesized in DEG, TREG, and GLY (as determined by analysis of the TEM micrographs) are 15 ± 4, 16 ± 5, and 25 ± 8 nm, respectively. These compare favorably with the crystallite sizes estimated from XRD data using the Scherrer formula (15.2, 21.0, and 21.2 nm for DEG, TREG, and GLY, respectively). The increase in particle size with increasing annealing temperature is consistent with our earlier observations in TEG.

Variations of the polyol process have been shown to yield nanostructured powders,[58,66] nanocomposites,[67] and high aspect ratio nanowires.[68] Likewise, the formation of nanowires and interconnected structures from nanoparticle aggregation is known.[65,69−72] However, the formation of interconnected and highly branched intermetallic nanowire networks in our system was unexpected. The only difference between these syntheses and the synthesis in TEG is the solvent; all other synthetic parameters remained unchanged. Clearly the solvent and its interaction with the growing nanoparticles contribute significantly to the dramatic difference in morphology. Some insight into the growth mechanism can be gained from analysis of the nanowire networks formed in EG (Figure 8). The inset in Figure 8 shows a well-formed nanowire network, along with discrete nanoparticles and small nanoparticle aggregates. The enlarged image in Figure 8 shows nanoparticles that appear to be coalescing into aggregates. This suggests that individual AuCu nanoparticles form initially and that the solvent does not stabilize the surface as well as TEG, allowing the surfaces to interact, coalesce, and grow into larger extended networks. High-resolution TEM shows that the nanowire networks are polycrystalline, and there is no evidence for oriented attachment, which is known to occur during nanoparticle aggregation in some other systems.[71] The exact reason for the difference in reactivity among TEG, TREG, DEG, and GLY is not yet known, but is most likely correlated with the number of coordinating groups available on the solvent molecules. TEG has more oxygen atoms available to coordinate to the nanoparticle surface, so it may stabilize the nanoparticles better than the solvents that contain fewer coordinating oxygen atoms.

The morphology of the intermetallic nanowire networks appears similar to that of Au nanowire networks recently reported by Ramanath et al.[65] In their report, Au nanowire networks form spontaneously through coalescence at room temperature without the use of templates or polymeric surface

(66) (a) Kurihara, L. K.; Chow, G. M.; Schoen, P. E. *Nanostruct. Mater.* **1995**, *5*, 607−613. (b) Yin, H.; Chow, G. M. *J. Mater. Res.* **2003**, *18*, 180−187.
(67) Chow, G. M.; Kurihara, L. K.; Kemner, K. M.; Schoen, P. E.; Elam, W. T.; Ervin, A.; Keller, S.; Zhang, Y. D.; Budnick, J.; Ambrose, T. *J. Mater. Res.* **1995**, *10*, 1546−1554.
(68) (a) Sun, Y.; Gates, B.; Mayers, B.; Xia, Y. *Nano Lett.* **2002**, *2*, 165−168. (b) Sun, Y.; Xia, Y. *Adv. Mater.* **2002**, *14*, 833−837. (c) Sun, Y.; Mayers, B.; Herricks, T.; Xia, Y. *Nano Lett.* **2003**, *3*, 955−960.
(69) Korgel, B. A.; Fitzmaurice, D. *Adv. Mater.* **1998**, *10*, 661−665.
(70) Tang, Z.; Kotov, N. A.; Giersig, M. *Science* **2002**, *297*, 237−240.
(71) He, T.; Chen, D.; Jiao, X. *Chem. Mater.* **2004**, *16*, 737−743.
(72) Mao, C.; Solis, D. J.; Reiss, B. D.; Kottmann, S. T.; Sweeney, R. Y.; Hayhurst, A.; Georgiou, G.; Iverson, B.; Belcher, A. M. *Science* **2004**, *303*, 213−217.

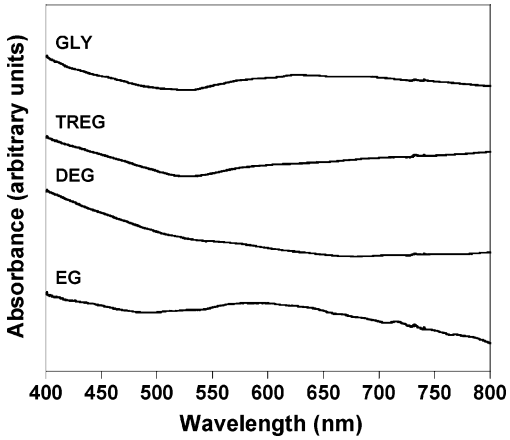

Figure 9. Visible absorption spectra for dilute solutions of AuCu nanowire networks synthesized in ethylene glycol (EG), diethylene glycol (DEG), triethylene glycol (TREG), and glycerol (GLY).

stabilizers.[65] Similar nanoparticle coalescence mechanisms have been exploited to form nanowires of metals[69] and semiconductors.[70] While our system is different, the similar results suggest that nanoparticle coalescence may be a general method for synthesizing self-supporting nanowire networks of complex solid-state materials. Our intermetallic nanowires also appear similar to those synthesized by Belcher and co-workers using biological templates.[72] In their study, virus-based scaffolds selectively template the formation of intermetallic FePt and CoPt nanowires.[72,73] Like our nanowire networks, the biologically templated nanowires tend to be highly branched and coiled.[72] The formation of similar nanowire networks from direct solution synthesis is interesting and shows that these complex morphologies can be accessed using different methods. Unlike the biologically templated intermetallic nanowires reported by Belcher and co-workers, however, ours are not single crystals.

The visible absorption spectra for dilute solutions of the AuCu nanowire networks are shown in Figure 9. The spectra for all of the nanowire networks show broad features without the sharp plasmon bands that were present for the discrete nanoparticles (Figure 5). The absorption spectrum for the partial nanowire network formed in EG at 198 °C (refer to Figure 8) shows several notable features. There is an absorption maximum near 580 nm, which could be due to either the AuCu alloy phase or pure Cu nanoparticles. Likewise, a weak absorption maximum around 520 nm matches that expected for pure Au nanoparticles, which are observed in the XRD data (Figure 6). Thus, the optical absorption spectrum for the nanowire network formed in EG is consistent with the presence of multiple types of nanoparticles, which are the precursors to the nanowire network that forms through nanoparticle coalescence. The visible absorption spectra for the other three nanowire networks (DEG, TREG, and GLY) appear similar, showing broad features between 400−475 nm and 550−700 nm. These spectra are clearly different from those of the discrete nanoparticles. Most notable is the region from 650 to 800 nm, which generally shows a constant or slightly

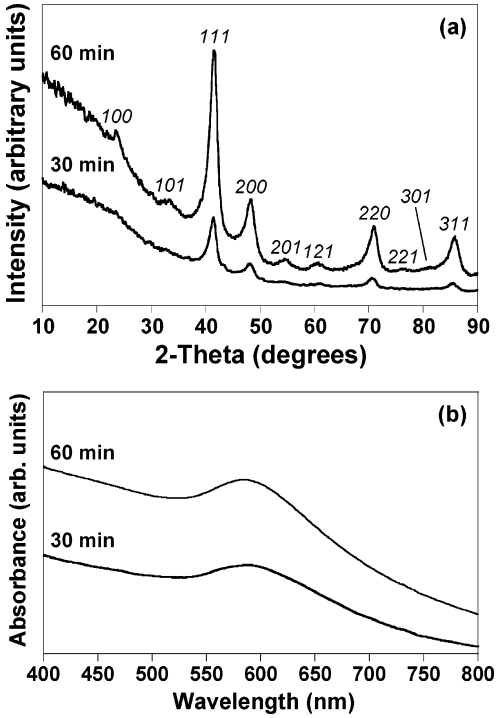

Figure 10. (a) Powder XRD patterns and (b) visible absorption spectra for $AuCu_3$ nanocrystals synthesized in tetraethylene glycol at 310 °C.

increasing absorbance. This is in contrast to the spectra of the discrete nanoparticles, which show a sharp drop in absorbance over this same range. The absorption features are consistent with those observed for coalescing Au nanoparticles[64] and Au nanowire networks of similar morphology,[65] specifically low-intensity plasmon bands, shifts to higher wavelengths, and broad bands in the 600−800 nm range.[64,65] These higher-wavelength bands have been attributed to longitudinal components of the surface plasmon, which are not usually observed unless aggregation occurs.[65]

Synthesis of Intermetallic $AuCu_3$ Nanocrystals. By adjusting the ratio of Au:Cu to between 1:2 and 1:3, nanocrystals of intermetallic $AuCu_3$ are formed. Figure 10 shows the time-dependent formation of $AuCu_3$ at 310 °C in TEG. Within 30 min, partially ordered $AuCu_3$ is observed. After 60 min, fully ordered intermetallic $AuCu_3$ is formed. (The slower rate of nucleation is consistent with what we observed in powder-based systems.[48]) Every reflection in the XRD pattern shown in Figure 10a can be indexed to the cubic $AuCu_3$ phase (a = 3.75 Å), which agrees well with the literature value (a_{lit} = 3.749 Å).[50] TEM micrographs and the corresponding size distribution histogram for the $AuCu_3$ nanocrystals are shown in Figure 11, and the SAED pattern confirms the ordered intermetallic structure. The visible absorption spectra in Figure 10b show a single plasmon band consistent with the formation of a single metallic phase. The absorption maxima near 575 nm are red-shifted slightly from those of AuCu, which is consistent with the higher concentration of Cu in $AuCu_3$ relative to AuCu.[39] The absorption maximum is essentially identical to that expected for pure Cu (rather than a Cu−Au alloy), and this likely results from the same effects that were discussed earlier for the AuCu samples. The TEM micrographs in Figure 11 show that the $AuCu_3$ nanocrystals are generally spherical, with average

(73) Reiss, B. D.; Mao, C.; Solis, D. J.; Ryan, K. S.; Thomson, T.; Belcher, A. M. *Nano Lett.* **2004**, *4*, 1127−1132.

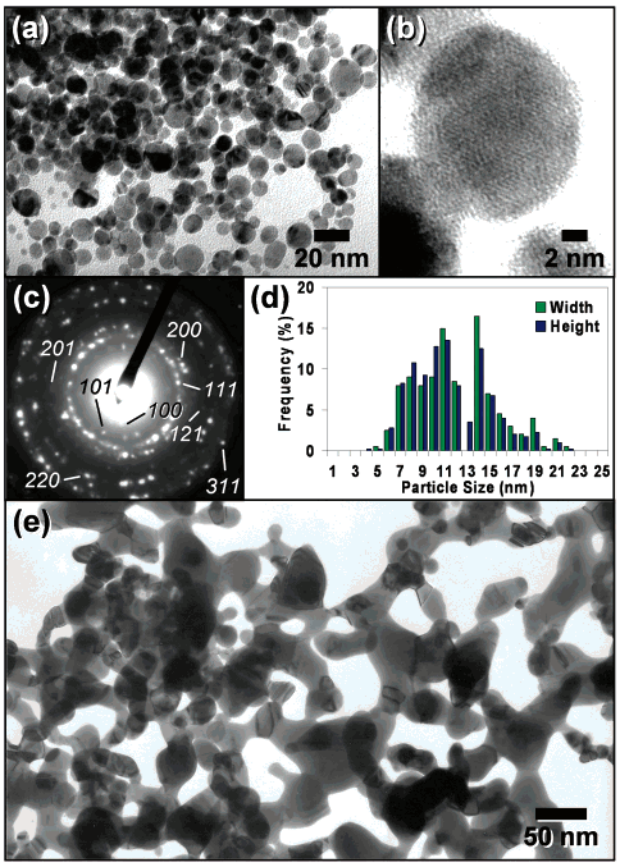

Figure 11. A TEM micrograph of $AuCu_3$ nanocrystals synthesized in tetraethylene glycol at 310 °C is shown in (a), and a high-resolution TEM micrograph of a single $AuCu_3$ nanocrystal is shown in (b). The corresponding size distribution histogram is shown in (d). A TEM micrograph of an $AuCu_3$ nanowire network synthesized in glycerol (290 °C) is shown in (e), along with the corresponding SAED pattern (c).

widths and heights of 11 ± 4 and 10 ± 3 nm, respectively. Note that the intermetallic $AuCu_3$ nanocrystals are generally more spherical than the intermetallic AuCu nanocrystals, and this may be influenced in part by the symmetries of the $AuCu_3$ (cubic) and AuCu (tetragonal) crystal structures. Clearly, this direct solution approach yields exquisite control over the composition and crystal structure of intermetallic nanocrystals. Furthermore, using glycerol as a solvent yields intermetallic $AuCu_3$ nanowire networks (Figure 11e), which shows that this solvent-based approach for accessing intermetallic nanomaterials with different morphologies is general in both composition and structure.

Conclusions

In this paper, we have established that intermetallic nanocrystals and nanowire networks can be synthesized directly in solution in a one-pot reaction. By correlating the solution annealing temperature and composition with the equilibrium phase diagram, the structure can be systematically tuned from disordered alloy to ordered intermetallic, and two distinct compounds, AuCu and $AuCu_3$, can be accessed as high-quality nanocrystals. Remarkably, the choice of solvent can be exploited to synthesize both nanocrystals and branched nanowire networks. The ability to simultaneously control structure, size, shape, and composition is unprecedented for intermetallic nanomaterials and has important implications both for fundamental scientific studies of structure−property relationships in complex nanomaterials and for future applications in catalysis,[74] biological sensing,[75] and nanoscale electronic and magnetic devices.[1,4,5,8] Extending this approach to other important intermetallic compounds of the late transition metals (e.g., FePt, CoPt) is feasible, because it is well-established that ordered intermetallic phases can nucleate at significantly lower temperatures using element substitution methods.[76]

The realization of large quantities of intermetallic nanocrystals using a one-step high-yield solution route lays the groundwork for a number of important scientific studies of fundamental physical phenomena at the nanoscale. For example, unresolved issues concerning the occurrence and size-dependence of phase transitions in nanocrystals[56,57] could be studied experimentally by analyzing size-selected nanocrystals synthesized using this direct solution approach. Issues of surface segregation, composition, structure, and reactivity in intermetallic nanocrystals are of paramount importance for catalysis and could be addressed experimentally for the first time, because large quantities of high-quality intermetallic nanocrystals were previously unavailable. This is especially important considering the recent interest in intermetallic compounds as superior catalytic materials.[12−15] Theoretical models of atomic ordering and crystallite morphology in intermetallic (especially Au−Cu) nanocrystals[51−55] could be tested experimentally using these nanocrystals. Finally, solution routes are known to influence the crystal structures of several classes of solid-state materials,[77] because surface interactions play a key role in structural stability and can be fine-tuned by judicious choice of ligands and solvent interactions. The direct solution route to intermetallic nanocrystals reported here could open the door to new metastable intermetallic structures with new or enhanced physical properties. Research aimed at extending this approach to other intermetallic systems, as well as fully exploring the physical properties, is currently in progress.

Acknowledgment. This work was supported by startup funds from Texas A&M University and funding from the Robert A. Welch Foundation (Grant No. A-1583). Acknowledgment is made to the Donors of the American Chemical Society Petroleum Research Fund for partial support of this research. Electron microscopy was performed at the Microscopy and Imaging Center at Texas A&M University. We thank Francois Gabbai for use of the UV−visible spectrophotometer.

CM0484450

(74) Schlogl, R.; Hamid, S. B. A. *Angew. Chem., Int. Ed.* **2004**, *43*, 1628−1637.
(75) Cai, H.; Zhu, N.; Ying, J.; He, P.; Fang, Y. *Biosens. Bioelectron.* **2003**, *18*, 1311−1319.
(76) (a) Kang, S. S.; Harrell, J. W.; Nikles, D. E. *Nano Lett.* **2002**, *2*, 1033−1036. (b) Kang, S. S.; Nikles, D. E.; Harrell, J. W. *J. Appl. Phys.* **2003**, *93*, 7178−7180. (c) Frommen, C.; Malik, S.; Wurfel, J. U.; Rosner, H.; Didschies, C. *Mater. Lett.* **2004**, *58*, 953−958.
(77) (a) Dinega, D. P.; Bawendi, M. G. *Angew. Chem., Int. Ed.* **1999**, *38*, 1788−1791. (b) Zhao, Y.; Zhang, Y.; Zhu, H.; Hadjipanayis, G. C.; Xiao, J. Q. *J. Am. Chem. Soc.* **2004**, *126*, 6874−6875.